CHEMISTRY OF MATERIALS
Article

Chem. Mater. **2009,** *21,* 3799–3809 3799
DOI:10.1021/cm9008943

Tailoring the Morphology of $LiCoO_2$: A First Principles Study

Denis Kramer and Gerbrand Ceder*

Department of Materials Science and Engineering, Massachusetts Institute of Technology, Cambridge, Massachusetts 02139

Received March 31, 2009. Revised Manuscript Received June 18, 2009

Surface energies of several low-index surfaces of layered $LiCoO_2$ are investigated as a function of the external lithium and oxygen chemical potentials by means of First Principles calculations in the generalized gradient approximation (GGA) to density functional theory (DFT), treating on-site electron correlation within the DFT+U framework. We find the set of surfaces contained in the equilibrium shape to be depending on environment. The (0001) and $(10\bar{1}4)$ surfaces are present for all reasonable values of the Li and O chemical potentials. The $(01\bar{1}2)$ surface, however, is stable only under oxidizing conditions. The equilibrium shape is sensitive to the equilibration environment because the thermodynamically favorable surface terminations and surface energies of the polar (0001) and $(01\bar{1}2)$ surfaces are a function of environment. This provides a lever to tailor the crystal shape according to application requirements (e.g., as active material in lithium-ion batteries).

Introduction

Being the de facto standard as cathodic active material in Li-ion batteries, layered $LiCoO_2$ has attracted immense attention since its introduction as an intercalation electrode material.[1] A high voltage and good rate capability are the main reasons for the commercial success.

Recently, the efforts to comply with the ever increasing demand for specific power, reduced recharge times, and better rate capabilities resulted in a trend to fabricate electrodes containing micro- or nanodispersed $LiCoO_2$ particles.[2] Because of this trend toward the nanoscale, surface properties and surface processes become a major concern. Moreover, not every crystal surface partakes in the uptake (release) of Li ions; the (0001) surface, which can occupy a large fraction of the total particle surface, is impermeable for Li ions because Li would need to pass through Co−O octahedra. Instead Li enters through other surfaces and diffuses purely two-dimensional in planes perpendicular to (0001).[3] Hence, understanding and control of the particle shape and the relative area of different surfaces can be useful in tailoring the rate performance. Moreover, identification of the relevant surfaces that are exposed to the electrolyte and their characteristics might help in devising better strategies to inhibit parasitic surface reactions.

$LiCoO_2$ crystallizes in a layered structure with alternating Li, O, Co, and O planes along the [0001] direction. Each individual plane has hexagonal symmetry; the symmetry of the crystal, however, is reduced by a relative shift of adjacent O−Co−O sheets, resulting in a rhombohedral structure with space group $R\bar{3}m$. The stacking sequence of the O−Co−O sheets is ABC, a configuration referred to as the O3 host.[4]

Traditionally, $LiCoO_2$ is synthesized by standard ceramic processing: firing at about 900 °C and grinding.[5] Several, alternative low temperature preparation routes exist (e.g., chemical lithiation,[6] sol−gel processes,[7] and laser ablation deposition[8]); all these syntheses, however, share a prolonged, final heat-treatment to obtain the electrochemically favorable layered phase. As final annealing is required to yield well crystallized $LiCoO_2$, a successful strategy for tailoring the morphology of the crystals has to account for the equilibrium thermodynamics shaping the crystals during annealing.

We investigate the morphology by means of Density Functional Theory (DFT) calculations embedded in a thermodynamic framework to identify low-energy surfaces. Where necessary, we will show the dependence of the surface energy on the environment and deduce surface phase diagrams. Finally, we will highlight the implications of environment dependent surface energies with respect to the morphology of the particles based on Wulff constructions.[9]

*To whom correspondence should be addressed. E-mail: gceder@mit.edu.

(1) Mizushima, K.; Jones, P.; Wiseman, P.; Goodenough, J. B. *Mater. Res. Bull.* **1980**, *15*, 783–789.
(2) Okubo, M.; Hosono, E.; Kim, J.; Enomoto, M.; Kojima, N.; Kudo, T.; Zhou, H.; Honma, I. *J. Am. Chem. Soc.* **2007**, *129*, 7444–7452.
(3) Van der Ven, A.; Ceder, G. *Electrochem. Solid-State Lett.* **2000**, *3*, 301–304.
(4) Delmas, C.; Fouassier, C.; Hagenmuller, P. *Phys. B C* **1980**, *99*, 81–85.
(5) Reimers, J. N.; Dahn, J. R. *J. Electrochem. Soc.* **1992**, *139*, 2091–2097.
(6) Fernandez-Rodriguez, J.; Morales, J.; Tirado, J. *Mater. Chem. Phys.* **1988**, *20*, 145–152.
(7) Kumta, P.; Gallet, D.; Waghray, A.; Blomgren, G.; Setter, M. *J. Power Sources* **1998**, *72*, 91–98.
(8) Antaya, M.; Dahn, J. R.; Preston, J.; Rossen, E.; Reimers, J. N. *J. Electrochem. Soc.* **1993**, *140*, 575–578.
(9) Cahn, J.; Carter, W. *Metall. Mater. Trans. A* **1996**, *27*, 1431–1440.

Published on Web 07/30/2009

Methodology

Surface Energy. Periodic boundary conditions, firmly integrated in most DFT codes that rely on a plane-wave basis set, make it natural to assess the energetics of surface formation by investigating sufficiently thick slabs. The periodicity in two dimensions ensures the infinity of the formed surface, and spurious interactions between slabs via the periodicity along the third dimension are quenched by sufficiently large gaps.

The surface energy of such a slab can be defined as the energy difference per unit surface area between the slab and the equivalent amount of each constituent in the bulk of the infinite solid. This leads to

$$\gamma = \frac{1}{2 \cdot A}\left(G_{\text{slab}} - \sum_{i \in \mathcal{S}} N_i \cdot \mu_i\right) \tag{1}$$

where i iterates through the complete set of species $\mathcal{S}=\{\text{Li, Co,O}\}$; the two surfaces of the slab are accounted for by dividing by $2A$, and N_i denotes the number of atoms of species i within the slab. The chemical potentials are not independent but have to sum to the free energy of the bulk compound g_b for a stoichiometric slab

$$g_b = \sum_{i \in \mathcal{S}} x_i \cdot \mu_i \tag{2}$$

where x_i is the number of atoms per formula unit of species i.

At this point, we assume the entropic and volumetric contributions to the free energy as negligible, and approximate the free energy g_b by the energy ε_b as obtained from DFT calculations. The surface energy for nonstoichiometric slabs depends on the environment as defined by the chemical potentials. This can be seen by rewriting eq 1

$$\gamma = \frac{1}{2 \cdot A}\left[E_{\text{slab}} - N_{\text{Co}}\left(\varepsilon_b - \sum_i \Gamma_i \cdot \mu_i\right)\right] \tag{3}$$

We choose Γ_i as the slab's excess of species i with respect to the stoichiometric composition per Co atom

$$\Gamma_i = \frac{N_i}{N_{\text{Co}}} - x_i \tag{4}$$

By choosing Co as the reference species, the chemical potential μ_{Co} always cancels exactly in eq 3 because Γ_{Co} equals zero by definition. Generally, Γ_i equals zero if the ratio of atoms of species i to the number of Co atoms is stoichiometric. Thus, the surface energy is constant for stoichiometric slabs, yet depends linearly on the chemical potential of oxygen and lithium otherwise. Note that this dependence on only two chemical potentials is not an approximation as only two independent chemical potentials can be defined in a ternary compound; the three chemical potentials have to sum to the energy of the compound.

Bounds for the Chemical Potentials. Meaningful limits for the chemical potentials are defined by the stability of the bulk structure as outside this range the surface energies are irrelevant.

Thus, the range of meaningful chemical potentials is essentially given by the area of the Li−Co−O phase diagram occupied by $LiCoO_2$. Upper limits are easily identified as defined by the pure elements, and we define these as the reference chemical potentials

$$\mu_i^* = E_i^0 \tag{5}$$

where E_i^0 denotes the energy per atom of the pure element. Metallic lithium and the gaseous oxygen dimer serve as reference states.

Lower bounds can be directly defined from the relation between the chemical potentials and the energy of the bulk compound ε_b (cf. Equation 2). Neither chemical potential must become so negative that at least one of the others has to be larger than the chemical potential of the pure elements. Thus, the valid range of chemical potentials (again neglecting entropic and volumetric work contributions) is given by

$$\varepsilon_f / x_i \leq (\mu_i - \mu_i^*) \leq 0 \tag{6}$$

The energy of formation ε_f is defined in the usual way as

$$\varepsilon_f = \varepsilon_b - \sum_{i \in \mathcal{S}} x_i \cdot \mu_i^* \tag{7}$$

a quantity that is negative for any stable compound. Equation 6 is a necessary but not sufficient condition for the bulk phase to be stable because it merely reflects the stability of the compound with respect to the pure reference states. Each equilibrium between stable phases in the ternary system and the compound imposes a similar condition, which is best visualized in a phase diagram.

Total Energy Calculations. Accurate total energy calculations of transition metal oxides within the DFT framework require the consideration of correlation effects, as well as careful examination of possible error cancellation with respect to the reference states. It is well-known that the general gradient approximation (GGA) to DFT does not always reflects the correlation effects of the 3d-electrons in transition metals with sufficient accuracy. This is particularly important when comparing equilibria in which electron transfer occurs, as in oxidation/reduction reactions, because of the lack of cancellation of the self-interaction.[10,11] It was shown recently by Wang et al. that the reasonable quantitative agreement between experimental reaction enthalpies of several transition metal oxides and those calculated in the GGA approximation largely originates from a coincidental cancellation of errors; the error in estimating the 3d-electron correlation energy is compensated by a combination of overestimating the oxygen dimer binding energy and a possible contribution associated with the addition of two electrons to the oxygen p-orbitals to form O^{2-} from O_2.[12]

We, therefore, follow the scheme proposed by Wang et al.,[12] treating 3d-electron correlation within the GGA+U framework[13−15] and including a correction term for the oxygen molecule derived by Wang et al.[12] for the calculation of formation energies and the reference chemical potential of oxygen. All total energy calculations were performed within the GGA+U approximation.[13−15] Projector augmented wave (PAW) pseudopotentials[16] were used, as implemented in the Vienna Ab Initio Simulation Package (VASP).[16,17] The rotationally invariant formulation of the on-site Hubbard-U model given by Dudarev et al.[18] was utilized at the Co sites

(10) Zhou, F.; Cococcioni, M.; Marianetti, C.; Morgan, D.; Ceder, G. *Phys. Rev. B* **2004**, *70*, 235121.
(11) Zhou, F.; Cococcioni, M.; Kang, K.; Ceder, G. *Electrochem. Commun.* **2004**, *6*, 1144–1148.
(12) Wang, L.; Maxisch, T.; Ceder, G. *Phys. Rev. B* **2006**, *73*, 195107.
(13) Anisimov, V. I.; Zaanen, J.; Andersen, O. K. *Phys. Rev. B* **1991**, *44*, 943–954.
(14) Anisimov, V. I.; Aryasetiawan, F.; Lichtenstein, A. *J. Phys.: Condens. Matter* **1997**, *9*, 767–808.
(15) Bacq, O. L.; Pasturel, A.; Bengone, O. *Phys. Rev. B* **2004**, *69*, 245107.
(16) Kresse, G.; Joubert, D. *Phys. Rev. B* **1999**, *59*, 1758–1775.
(17) Kresse, G.; Furthmüller, J. *Phys. Rev. B* **1996**, *54*, 11169.
(18) Dudarev, S. L.; Savrasov, S. Y.; Humphreys, C. J.; Sutton, A. P. *Phys. Rev. B* **1998**, *57*, 1505–1509.

as implemented in VASP for all calculations. The on-site Hubbard-U model was parametrized with $U - J = 3.3$ eV originating from a fit to experimental oxidation energies of cobalt oxides.[12]

We found a k-point mesh of $6 \times 6 \times 6$ sufficiently dense for the bulk unit cell (i.e., the reduced cell with four atoms). The slabs were covered with a similarly dense k-point mesh in reciprocal space only parallel to the surface to minimize spurious interactions with super cell images. All calculations were performed with a plane wave cut off of 550 eV. The volume of all slab unit cells was fixed to a geometry equivalent to the fully relaxed bulk, and only the atomic coordinates were allowed to relax. This approach is similar to the one recently used to calculate the surfaces of $LiFePO_4$[19] and $LiMnPO_4$.[20]

Selected Surfaces and Terminations. The selection of surfaces to investigate was limited to low-index surfaces and guided by favoring surfaces with minimal coordination loss of Co. It was found in previous work on related compounds that coordination loss of the transition metal creates high energy surfaces.[19] This led to the following set of surfaces: (0001), $(11\bar{2}0)$, $(10\bar{1}0)$, $(01\bar{1}2)$, and $(10\bar{1}4)$. We use hexagonal notation to denote the surfaces as it is easy to visualize. Although redundant, the introduction of an addition index as the third digit makes it easier to identify surfaces related by symmetry in hexagonal lattices.[21] The reader should, however, consider that the space group of $LiCoO_2$ is $R\bar{3}m$. Thus, the usual hexagonal 6-fold rotational symmetry cannot be applied in general to find the full form that each of these surfaces represent (i.e., the set of all symmetry equivalent surfaces). The {0001} form contains just the $(000\bar{1})$ surface in addition to (0001). The $\{11\bar{2}0\}$ and $\{10\bar{1}0\}$ forms contain six equivalent surfaces; all of them can be found by the usual index permutation and inversion. Yet, only six, out of the twelve surfaces that can be found by index permutation and inversion, are crystallographically equivalent for $\{01\bar{1}2\}$ and $\{10\bar{1}4\}$. These are $(01\bar{1}2)$, $(1\bar{1}02)$, $(\bar{1}012)$, $(10\bar{1}\,\bar{2})$, $(\bar{1}10\bar{2})$, and $(0\bar{1}1\bar{2})$ for $\{01\bar{1}2\}$, and $(10\bar{1}4)$, $(\bar{1}104)$, $(0\bar{1}14)$, $(1\bar{1}0\bar{4})$, $(01\bar{1}\,\bar{4})$, and $(\bar{1}01\bar{4})$ for $\{10\bar{1}4\}$.

Nonpolar Surfaces. Among the investigated surfaces, the $(11\bar{2}0)$, $(10\bar{1}0)$, and $(10\bar{1}4)$ surfaces are nonpolar. Illustrations of these surfaces are given in Figure 1. According to Tasker,[22] oxide surfaces can be classified based on the dipole moment and charge of the repetitive unit parallel to the surface assigning to each atomic position a point charge with the respective formal valence. The Tasker classification, therefore, is solely based on electrostatic arguments and leads to three classes of surfaces: type I surfaces are characterized by zero charge ($q = 0$) and dipole moment ($\mu = 0$) per repetitive unit. Type II surfaces are defined by zero dipole moment per repetitive unit, yet each individual layer may possess a finite charge. Naturally, the charges of the individual layers have to compensate each other, leading to zero net charge per repetitive unit. Finally, type III surfaces are characterized by a finite dipole moment per repetitive unit. Formally, cleavage of these polar surfaces leads to an infinite surface energy (based on purely electrostatic considerations).

The $(11\bar{2}0)$ and $(10\bar{1}0)$ surfaces belong to Taskers type I; each layer is composed of all three species in a stoichiometric ratio,

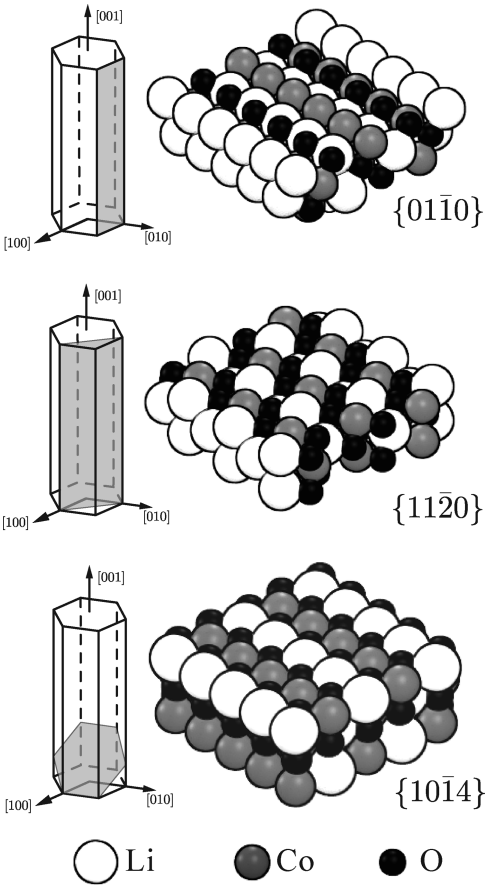

Figure 1. Illustration of the cleavage plane and sphere model of the investigated nonpolar surfaces; the $\{01\bar{1}0\}$ and $\{11\bar{2}0\}$ surfaces cleave the crystal perpendicular to the Li planes and in an angle of $\pi/3$ to each other; the $\{10\bar{1}4\}$ surfaces cleave the crystal in an angle such that the surface Co is 5-fold coordinated.

leading to zero dipole moment and net charge. Moreover, the termination for these surfaces is unambiguously defined because all layer are equivalent. Strictly speaking, the $(10\bar{1}4)$ surfaces belong to Taskers type II. If a plane cutting through the Li and Co atoms is envisioned, the O atoms form separate, slightly offset layers, parallel to the Li−Co plane. Thus, the repetitive unit is O−(Li,Co)−O, which leads to formally doubly charged planes yet zero dipole moment perpendicular to the surface. The distance between two adjacent O−(Li,Co) planes, however, is practically negligible, and the $(10\bar{1}4)$ surfaces can be understood as type I surfaces, again with an unambiguously defined termination.

Finally, all these cleavage planes comprise a stoichiometric ratio of the constituents. Thus, the surfaces are readily modeled as slabs, having equal surfaces on both sides of the slab and containing a stoichiometric ratio of constituents. Recalling eq 3, this leads to a uniquely defined surface energy, independent of the environment.

Stabilizing Polar Surfaces. In addition to the three nonpolar surfaces, two polar surfaces were investigated: the (0001) and $(01\bar{1}2)$ surfaces. The cleavage planes and repeat units of both surfaces are depicted in Figure 2. Cleaving the crystal along both planes leads to a dipole within the repeat unit; the (0001) plane results in a lithium plane with formal charge $q = +1$ contrasted by a O−Co−O plane with a formal sum charge of $q = -1$, and the repeat unit for the $(01\bar{1}2)$ plane consists of two layers with formal charge +4 (cation plane with Li and Co) and −4 (oxygen plane).

(19) Wang, L.; Zhou, F.; Meng, Y. S.; Ceder, G. *Phys. Rev. B* **2007**, *76*, 1–11.
(20) Wang, L.; Zhou, F.; Ceder, G. *Electrochem. Solid-State Lett.* **2008**, *11*, A94–A96.
(21) Buerger, M. J. *Elementary Crystallography: An Introduction to the Fundamental Geometrical Features of Crystals*; MIT Press: Cambridge, MA, 1978.
(22) Tasker, P. *J. Phys. C: Solid State Phys.* **1979**, *12*, 4977–4984.

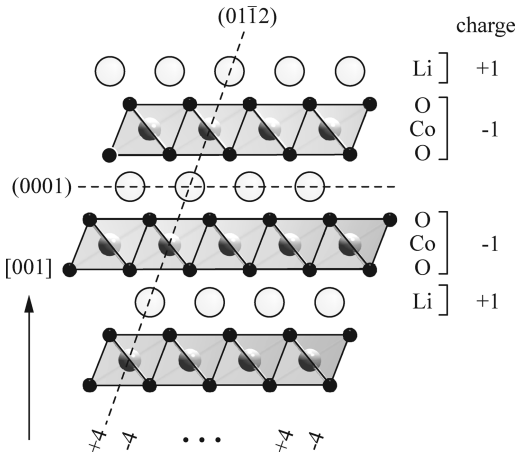

Figure 2. Illustration of cleavage planes leading to polar surfaces. Color coding of atoms as in Figure 1.

Generating a stoichiometric slab for assessing the surface energy of polar surfaces by simply cleaving the crystal gives rise to erroneous results because the formation of a noncompensated surface layer would result in a finite electric field throughout the crystal.[22] The key to stabilizing polar surfaces is the redistribution of charge in the terminating surface layers while maintaining global charge balance. To obtain a finite surface energy that does not scale with slab thickness, the electric fields generated by both terminating surface layers have to compensate each other exactly. Furthermore, both surfaces have to be equal to assign a surface energy to the chosen termination.

Different degrees of freedom can be utilized to achieve the cancellation, which essentially amounts to generating symmetrical, equally charged terminating layers. The illustrations depicted in Figure 3 exemplify the different basic compensating measures available for the (0001) surface. First, the slab can be terminated by half a monolayer (ML) lithium on both sides of the slab, as shown in illustration a of Figure 3. This leads to an equal charge of $q = +1/2$ for both surface layers. Moreover, this configuration ensures global neutrality of the slab—even in the simplified ionic model. Each electron liberated from a lithium atom is matched by an accommodating Co t_{2g}-state leading to a formal valence of +3 for each Co. Second, the slab can be terminated by O−Co−O layers on both sides, a configuration shown as b in Figure 3. In this lithium deficient configuration, the surface O−Co−O layers have to accommodate a sum charge of $q = -1/2$ each to ensure global neutrality of the slab, leading to either a mixed valence of the Co ions (i.e., an equal number of Co^{4+} and Co^{3+} ions) or delocalized electrons in the surface layer. Finally, termination by an oxygen deficient O−Co−O layer can likewise provide compensating charges of the surface layers and maintain global neutrality; removal of 1/4 of the oxygen atoms at the surface ensures global neutrality if a cobalt valence of Co^{3+} prevails throughout the slab.

Cleavage along the (01$\bar{1}$2) plane results in alternating anion and cation layers below the (01$\bar{1}$2) surface. Every symmetrical termination by anion or cation layers cancels the electric fields of the surface layers. Undercoordinated Co at the surface, however, is energetically costly as will be shown later, and termination of the (01$\bar{1}$2) surface by anion layers is more likely to yield stable surfaces than termination by cation layers. In this case, each surface layer has to provide a sum charge of $q = -2$ for the slab to be charge balanced. Thus, removal of every second oxygen atom from the terminating surface layers is needed (i.e., 1/2 ML oxygen coverage) for Co^{3+} to prevail throughout the slab. A different oxygen coverage is only possible if global charge balance is restored by other means.

Results

Chemical Potential Limits on Bulk $LiCoO_2$. We calculated the formation energies of a series of Li−Co−O compounds within the GGA+U approximation parametrized with $U - J = 3.3$ eV. The set of considered compounds comprises those already identified as stable by Wang et al.[12] In addition, we considered five partially lithiated, layered Li_xCoO_2 compounds, using previously identified low-energy lithium arrangements.[23] The respective formation energies of stable compounds are given in Table 1. Our results agree with those of Wang et al. despite the different parametrization of the on-site Hubbard-U. They parametrized their calculation with a larger U-value derived from self-consistent calculations instead of fitting to experimental data.

The resulting phase equilibria within the ternary Li−Co−O system are summarized in Figure 4. The plot shows the phase relations within the system as a function of the chemical potentials of lithium μ(Li) and oxygen μ(O). Because metallic Li was chosen as reference state μ^*(Li), the scale of the Li chemical potential translates directly into the negative of the voltage against $Li|Li^+$. The oxygen dimer at 0 K sets the reference state for the oxygen chemical potential, the dashed line marking the stability limit against gaseous oxygen at 0 K. Compounds with a stability window solely above this line, most notably fully delithiated, layered CoO_2, are thermodynamically not stable at 0 K. Note that the chemical potential of gaseous oxygen is a function of pressure and temperature. Hence, the dashed line only marks the phase stability against gaseous oxygen at 0 K. Gaseous oxygen at room temperature and ambient pressure, for example, would set a limiting chemical potential approximately 0.2 eV below μ^* (O); this estimate is based on the free energy of an ideal gas using the Sackur−Tetrode equation to account for entropic contributions. As the phase rule requires, the existence of two-phase equilibria is marked by lines, and invariant points form where three compounds coexist. Compounds that contain no Co are represented as lines rather than areas in this plot because of the independence on the cobalt chemical potential, which restricts the number of independent chemical potentials to one. Binary compounds that do not contain Li are still represented by an area because the oxygen chemical potential for these compounds is independent of the lithium chemical potential.

The absence of partially delithiated, layered Li_xCoO_2 phases from the phase diagram shown in Figure 4 is in accordance with the experimentally observed meta-stability of these compounds.[26] In an oxidizing atmosphere,

(23) Wolverton, C.; Zunger, A. *Phys. Rev. Lett.* **1998**, *81*, 606–609.
(24) Barin, I. *Thermochemical Data of Pure Substances*, 2nd ed.; VCH: Weinheim, Germany,1993.
(25) Styer, D. *Am. J. Phys.* **2000**, *68*, 1090–1096.
(26) Baba, Y.; Okada, S.; Yamaki, J. *Solid State Ionics* **2002**, *148*, 311–316.

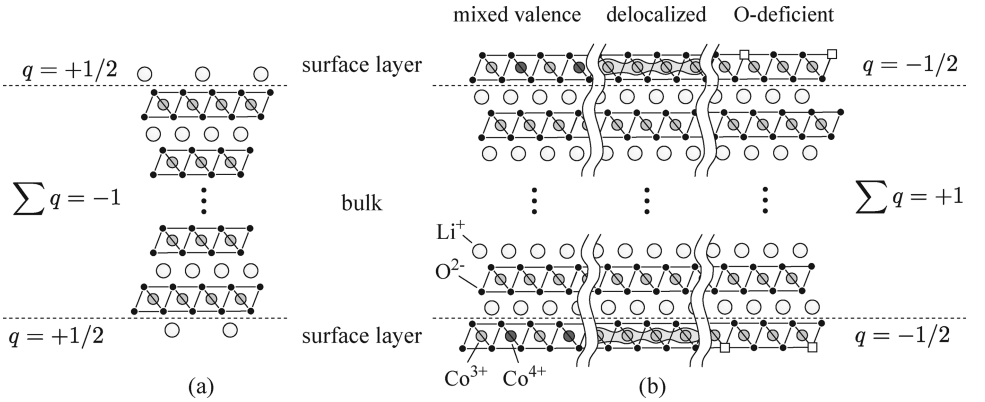

Figure 3. Surface terminations for the polar (0001) surface that ensure global charge balance and compensating electric fields of the surface layers: (a) shows termination by 1/2 ML of Li^+; sketch (b) depicts different terminations by O−Co−O layers.

Table 1. Calculated Lattice Constants and Formation Energies ε_f of Stable Bulk Compounds in the Li−Co−O System

compound	structure	space group	a [Å]	b [Å]	c [Å]	ε_f [eV/atom]
CoO	rocksalt	$Fm\bar{3}m$	4.272	4.272	4.272	−1.235[a]
Co_3O_4	spinel	$Fd\bar{3}m$	8.141	8.141	8.141	−1.394
CoO_2	layered O1	$P\bar{3}m1$	2.900	2.900	4.359	−1.076
$LiCoO_2$	layered O3	$R\bar{3}m$	2.826	2.826	14.207	−1.780
$LiCo_2O_4$	spinel	$Fd\bar{3}m$	8.031	8.031	8.031	−1.516
Li_2O	fluorite	$Fm\bar{3}m$	4.636	4.636	4.636	−2.093
Li_2O_2	hexagonal	$P6_3/mmc$	3.168	3.168	7.688	−1.760

[a] CoO serves as reference species, and the experimental formation energy used from Barin et al.[24] is given.

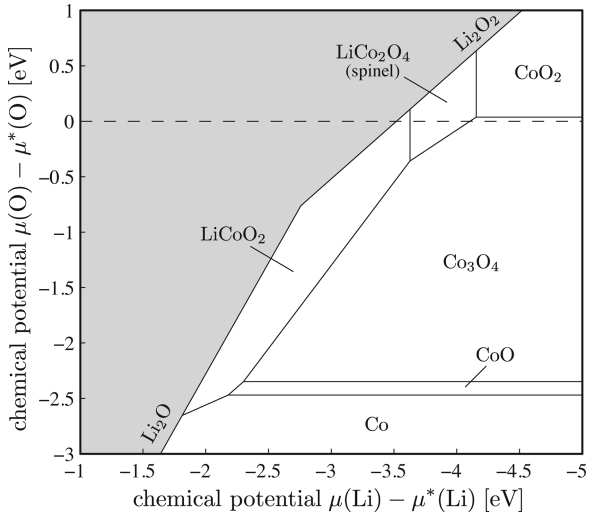

Figure 4. Phase diagram of the Li−Co−O system in chemical potential space showing the stability region of bulk $LiCoO_2$.

the conversion to the spinel Co_3O_4 and cation-mixed spinel $LiCo_2O_4$ set the lower limit of the chemical potential of lithium (upper voltage against $Li|Li^+$) at which the bulk phase is thermodynamically stable. This is likewise in agreement with experiment, where spinel structures were found as decomposition products of partially delithiated Li_xCoO_2.[27,28] Interestingly, voltages as low as 2.0−2.5 V suffice under strongly reducing conditions

Table 2. Terminations and Surface Energies of the Nonpolar Surfaces[a]

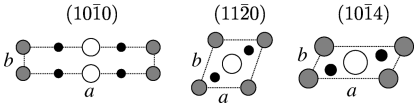

surface	a [Å]	b [Å]	$\angle(a,b)$ [deg]	coord.	γ[mJ/m^2]
(10$\bar{1}$0)	14.04	2.814	90.0	3/5	2943
(11$\bar{2}$0)	4.874	4.955	70.9	4/6	2241
(10$\bar{1}$4)	6.355	2.814	63.7	5/6	1048

[a] The illustrations depict the surface unit cells with Li represented by white, Co by gray, and O by black circles; also given is the Co−O coordination number within the surface layer and the first sublayer.

to stabilize Co_3O_4, CoO, or metallic Co. All three compounds were found as decomposition products of partially delithiated Li_xCoO_2 in contact with organic solvents,[29] the solvent being the reducing agent. Overlithiation leads to the formation of Li_2O under reducing and Li_2O_2 under oxidizing conditions, both defining the upper stability limit with respect to the chemical potential of lithium (lower limiting voltage) for a given oxygen chemical potential. Among the overlithiation reactions discussed by Benedek et al.,[30] only the formation of metallic cobalt leads to a three-phase equilibrium with Li_2O according to Figure 4.

Energetics of Surface Formation. *Nonpolar surfaces.* For Tasker-Type I surfaces, the surface energy is independent of the environment if each atomic layer beneath the surface is stoichiometric. All investigated nonpolar surfaces belong to this class. Comprising a stoichiometric ratio of atoms, each individual atomic layer parallel to the surface is charge balanced. Strictly speaking, this is only true for the unrelaxed, freshly cleaved surface. Nonetheless, only one termination per nonpolar, stoichiometric surface is possible for a stoichiometric slab of $LiCoO_2$. The 2D unit cells for the nonpolar surfaces are given in Table 2, together with the calculated surface energies. With 1048 mJ/m^2 the (10$\bar{1}$4) surface energy is lowest and is only about half as high as the surface

(27) Yamaki, J.; Baba, Y.; Katayama, N.; Takatsuji, H. *J. Power Sources* **2003**, *119−121*, 789–793.
(28) Dahn, J. R.; Fuller, E.; Obrovac, M.; Sacken, U. V. *Solid State Ionics* **1994**, *69*, 265–270.
(29) MacNeil, D. D.; Dahn, J. R. *J. Electrochem. Soc.* **2002**, *149*, A912–A919.
(30) Benedek, R.; Vaughey, J.; Thackeray, M. M. *Chem. Mater.* **2006**, *18*, 1296–1302.

energy obtained for $(11\bar{2}0)$. The $(10\bar{1}0)$ surface has the highest energy among the nonpolar surfaces considered.

These surface energies can be rationalized in terms of the coordination loss. It appears reasonable to assume that the surface energy can largely be attributed to the breaking of Co−O bonds upon cleavage, similar to what was found for Fe in $LiFePO_4$.[19] Indeed, a strong linear trend is observed if the cleavage energy is plotted as a function of coordination loss. This suggests that the cleavage energy can be modeled by

$$\Delta E_{\mathrm{cl}} = \gamma \cdot 2A \tilde{=} \Delta E_{\mathrm{c}} \sum_i \xi_i + \Delta E_{\mathrm{r}} \qquad (8)$$

where the coordination loss of the i-th Co atom is denoted as ξ_i, with the sum running over all undercoordinated Co. The last term ΔE_{r} absorbs the remaining contributions to the surface energy such as the energy gain from relaxing the surface atoms after cleavage. A coordination loss energy of $\Delta E_{\mathrm{c}} = 1.027 \pm 0.016$ eV is found per Co−O bond lost from a least-squares fit of eq 8 to the surface energies given in Table 2. ΔE_{r} amounts to -0.118 ± 0.011 eV per surface atom. This unveils that nonpolar low energy surfaces are characterized by a minimal coordination loss of surface Co, and it is worth pointing out that cleavage along the $(10\bar{1}4)$ plane is the only possibility yielding a coordination loss of one. Zero coordination loss is achievable by cleaving along the (0001) and $(01\bar{1}2)$ planes; yet, this leads to polar surfaces where the simple model represented by eq 8 does not hold.

Polar $(01\bar{1}2)$ *Surface*. As already mentioned and illustrated in Figure 2, the $(01\bar{1}2)$ plane consists of alternating cation/oxygen planes, allowing for termination by either plane. In both cases, however, the resulting slab is not charge-balanced if it is terminated by fully occupied surface planes. Among the two possibilities for creating a charge-balanced and stoichiometric slab, the termination by 1/2 ML of oxygen at the surface will be energetically more favorable compared to a partially vacant cation surface layer based on the findings in the last paragraph. Thus, we focus on (partial) oxygen terminations to elucidate the energetics of the surface. The unit cell of the oxygen surface plane is rectangular and provides two distinct sites for oxygen; oxygen at the A site has two Co and one Li as nearest neighbors in the first cation layer below the surface. The ratio is reversed for the B site (cf., sketches of Figure 5). The rectangular lattice can be seen as a distorted hexagonal lattice; the distortion being a result of the different ionic radii of the cation rows beneath the oxygen layer.

The plot of Figure 5 shows the surface energy of the $(01\bar{1}2)$ surface with 1/2 ML oxygen termination for different oxygen superstructures. Three configurations are compared: in configuration a every A site is occupied, every second A and B site is occupied in b, and occupation of the B sites only results in configuration c. These configurations are characterized by a different coordination loss of the Co atoms in the first cation layer. Each Co is 5-fold coordinated in the first cation layer for

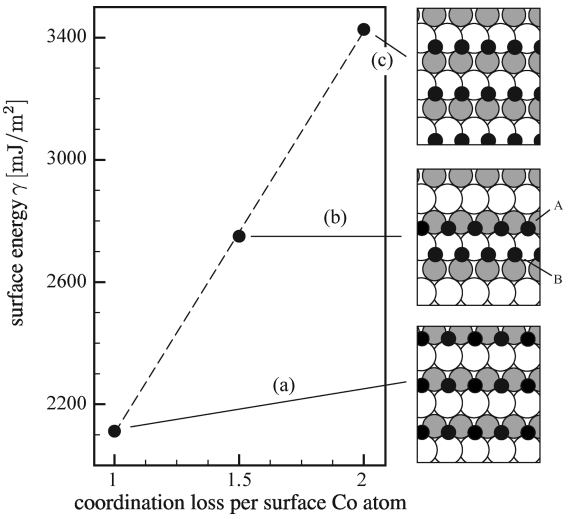

Figure 5. Surface energy of the $(01\bar{1}2)$ surface terminated by 1/2 ML of oxygen as a function of Co coordination loss; the different surface configurations are sketched to the right, where oxygen is indicated by black, Li by white, and Co by gray circles.

configuration a and 4-fold coordinated in c. Configuration b is a mixture of a and c in the sense that equal amounts of 4-fold and 5-fold coordinated Co are present, leading to an average coordination loss of 1.5. The linear dependence of the surface energy on the average coordination loss seen in Figure 5 corroborates the conclusions derived from investigating the nonpolar surfaces: the coordination loss of Co dominates the surface energetics for stoichiometric slabs and its minimization provides the leading principle to generate low-energy surfaces. A coordination loss energy of 1.145 ± 0.046 eV can be inferred from the slope of the linear trend. This value is in reasonable agreement with the coordination loss energy found previously for the nonpolar surfaces. The absolute value of the surface energy, however, is significantly larger than for a nonpolar surface with the same coordination loss. This indicates that an additional energy of about 1 eV per Co atom in the first cation layer contributes to the surface energy of the $(01\bar{1}2)$ surface. This energy might arise from the reduced screening of the coulomb repulsion between cations where an oxygen vacancy is formed.

The surface energy of the $(01\bar{1}2)$ surface can be lowered under strongly oxidizing (reducing) conditions by increasing (decreasing) the oxygen surface coverage. As expressed by eq 3, the surface energy depends linearly on the oxygen chemical potential for nonstoichiometric configurations. This is reflected in Figure 6, which shows the surface energy for different oxygen surface coverages as a function of the oxygen chemical potential. We find four superstructures to be stable depending on the oxygen chemical potential. The stoichiometric occupation of each A site (1/2 ML) has a stability window ranging from about -1.5 to -2.25 eV. If the environment sets a less negative chemical potential (i.e., becomes more oxidizing), then each second B site becomes occupied, stabilizing a superstructure equivalent to a surface coverage of 3/4 ML. Terminating the surface by a full monolayer of oxygen provides the lowest surface energy under

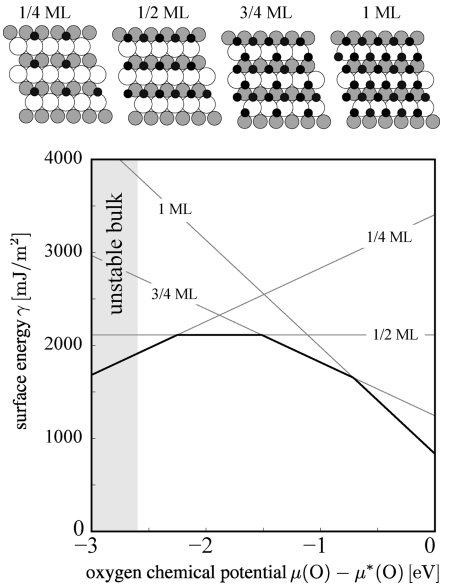

Figure 6. Surface energy of the oxygen terminated $(01\bar{1}2)$ surface as a function of oxygen chemical potential; the lower envelope giving the respective stable oxygen surface coverage is emphasized as thick black line; the sketches above the plot show the respective superstructures with the same color coding of the atoms as in Figure 5.

oxidizing conditions (μ(O) > −0.7 eV). In a reducing atmosphere, a rather small stability window for the occupation of every second A site (1/4 ML) exists before the bulk stability limit is reached. Thus, the surface energy of the $(01\bar{1}2)$ surface can be lowered to values comparable to the $(10\bar{1}4)$ surface, the lowest energy nonpolar surface, under highly oxidizing conditions. In reducing atmosphere, it is not feasible to lower the surface energy of the $(01\bar{1}2)$ surface due to the limiting bulk stability.

We have argued earlier that a charge balanced slab with $(01\bar{1}2)$ surfaces requires 1/2 ML of oxygen coverage if Co^{3+} prevails throughout the slab. Therefore, a higher surface coverage of oxygen, where B sites are occupied, implies a mechanism to restore global charge balance. The charge density plot in Figure 7 confirms the mechanism at hand: the charge compensation is achieved by emptying t_{2g} states of the Co ions in the first cation layer beneath the surface, which corresponds to the presence of Co^{4+} within this layer. The plot shows the difference in charge density between a $(01\bar{1}2)$ surface with every B site vacant (cf., Figure 5) and a fully occupied oxygen layer at the surface. A dashed line in the inset, which shows a side view sketch, indicates the plane of the charge density plot. An increase in electron density (i.e., a more negative charge density) is shown as light-gray to white, while a decrease in electron density is shown as dark-gray to black. A slight, secondary redistribution of charge at the second oxygen row can be seen in Figure 5 beside the redistribution of charge from Co in the first cation layer toward the additional surface oxygen. Yet, no change of the charge density is found beyond that layer, showing that global charge compensation is ensured locally near the surface and can be interpreted in terms of the ionic model developed earlier.

Polar (0001) surface. The second low-index surface sensitive to the environment is the polar (0001) surface. As illustrated in Figure 2, this surface is created by cleaving the crystal parallel to the Li plane. In principle, the crystal can be terminated along this plane in three layers: the Li layer, the Co layer, and either of the oxygen layers. This surface was already studied by means of DFT calculations by Hu et al.,[31] who restricted their considerations to stoichiometric slabs. They found the termination by surface Co highly unfavorable compared to terminating the slab with 1/2 ML of Li on each side. This agrees with our general findings.

Thus, our investigation is limited to (partial) Li terminations and (partial) oxygen terminations with a Co layer being the first cation layer beneath the surface. Nonetheless, a full surface phase diagram is a formidable task given the large number of possible atomic arrangements of partially occupied terminating layers (superstructures). In principle, one needs to investigate a forbiddingly large set of Li/vacancy and O/vacancy orderings. We, therefore, decided to constrain our search for stable Li superstructures to orderings that are equal or similar to stable orderings in the Li layers of partially delithiated bulk Li_xCoO_2.[23] This yielded a set of about 20 different Li superstructures that were calculated. Our search for O/vacancy orderings was even less extensive (about 10 different superstructures) because oxygen vacancies imply the presence of energetically unfavorable, undercoordinated Co, making it unlikely that these surfaces yield lower surface energies than (partial) Li terminations within the limits of the bulk stability.

Even though this seems a rather limited set of configurations, it still yields a substantial set of calculations because different charge orderings of mixed valence Co in the first sublayer have to be taken into account as well. In the case of a Li terminated surface, global charge balance requires 1/2 ML of Li surface coverage (cf., Figure 3) if Co^{3+} prevails throughout the slab. Thus, a lower (higher) surface coverage implies the presence of a matching number of Co^{4+} (Co^{2+}) in the first Co layer in order to restore global charge balance. This introduces another degree of freedom because the different valences can be attributed to different Co atoms. However, it is reasonable to assume that the ordering of different valences on the Co atoms is largely due to electrostatics. Therefore, we calculated the Ewald sum of different Co valence orderings and initialized the DFT calculations with the ordering yielding the lowest Ewald sum. If the lowest Ewald sum was degenerate, we run multiple DFT calculations for a given Li ordering.

The surface phase diagram displayed in the lower part of Figure 8 summarizes our findings. The plot shows the terminations resulting in the lowest surface energy for a given environment together with the stability limits of the bulk structure according to Figure 4. We find that neither of the considered oxygen terminations has a stability

(31) Hu, L.; Xiong, Z.; Ouyang, C.; Shi, S.; Ji, Y.; Lei, M.; Wang, Z.; Li, H.; Huang, X.; Chen, L. *Phys. Rev. B* **2005**, *71*, 125433.

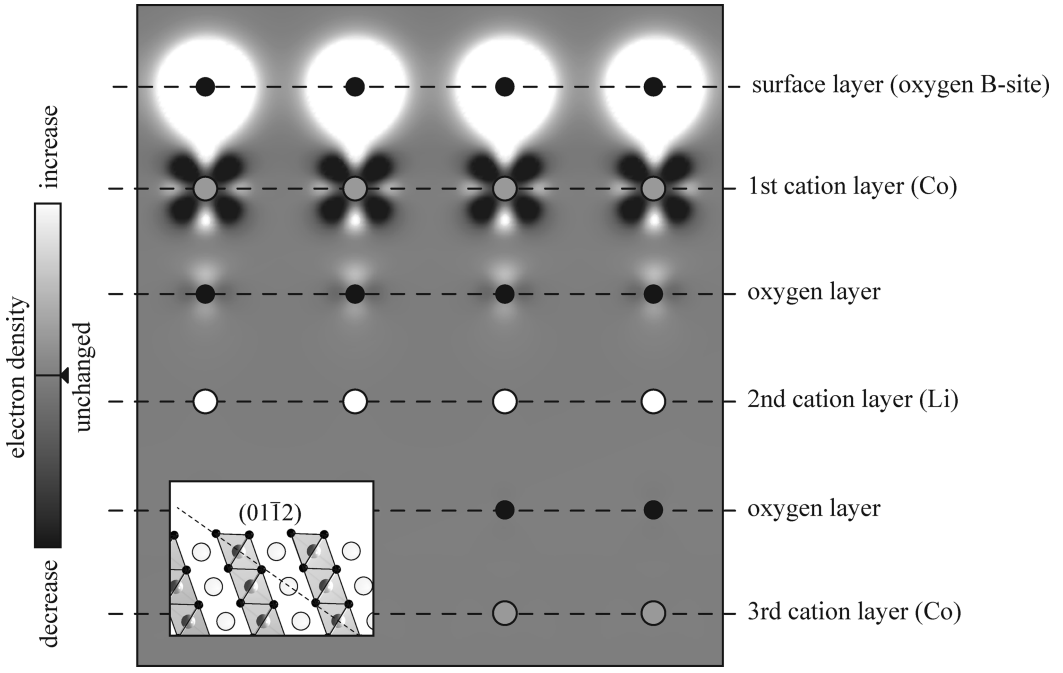

Figure 7. Charge density difference at the (01$\bar{1}$2) surface; the difference map refers to the charge density difference between a surface with every oxygen B site vacant, corresponding to configuration a in Figure 5, and a surface with full oxygen coverage.

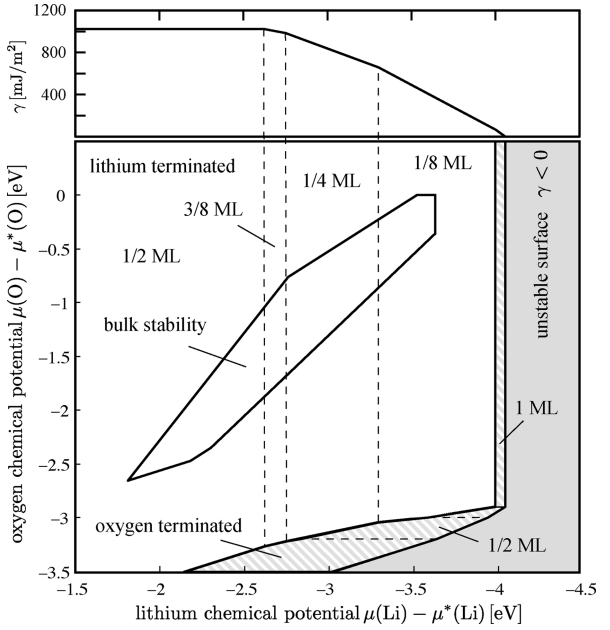

Figure 8. Surface phase diagram of the (0001) surface and corresponding surface energies for (partial) lithium terminations; (partial) lithium terminations are shown as white and stripes indicate (partial) oxygen terminations; see Figure 4 for bulk stability.

region that overlaps with the bulk stability window. A significantly more reducing environment than the bulk structure can sustain would be needed to stabilize any of the considered oxygen terminations. Therefore, the surface energy of the (0001) surface becomes an explicit function of the lithium chemical potential μ(Li) only as plotted in the upper diagram of Figure 8. The bulk stability window overlaps with four superstructures. Terminating the surface by 1/2 ML of Li atoms provides the lowest surface energy for chemical potentials μ(Li) ranging from −1.8 to −2.6 eV. By lowering μ(Li) (i.e., increasing the voltage) three more Li superstructures can be stabilized. The lithium coverage is reduced by first stabilizing a structure that corresponds to 3/8 ML coverage before a region that corresponds to 1/4 ML coverage is accessed. Finally, our results indicate that a superstructure occupying 1/8 of the available Li sites can form for μ(Li) < −3.3 eV. Within the limits of bulk stability, the surface energy of (0001) can, therefore, vary from about 1000 mJ/m^2 at high lithium chemical potentials to approximately 400 mJ/m^2 at low lithium chemical potentials.

The fact that only surfaces with ≤1/2 ML Li coverage share a stability region with the bulk can be rationalized by the redox potential of Co. The configurations depicted in Figure 3 constitute the range of configurations that allow for Co^{3+} throughout the slab. Thus, a Li coverage of 1/2 ML results in a charge balanced configuration with Co^{3+} prevailing throughout the slab, and more (less) Li^+ on the surface requires creation of Co^{2+} (Co^{4+}). In particular, reduction to Co^{2+} in the host is energetically unfavorable.

Crystal Shape. The sensitivity of the surface energy of the polar surfaces with respect to the environment provides a handle to tailor the equilibrium crystal shape. Controlling the oxygen chemical potential during annealing is straightforward by adjusting the oxygen partial pressure, the temperature, or by using a reducing agent such as hydrogen. The lithium chemical potential, however, is less amendable to experimental adjustment and can only be controlled indirectly by choosing the phases $LiCoO_2$ is in equilibrium with. For example, modifying the lithium to cobalt ratio away from stoichiometry can make $LiCoO_2$ coexist with other phases. If $LiCoO_2$ coexists with another phase, a linear relation between the lithium and oxygen chemical potentials is established.

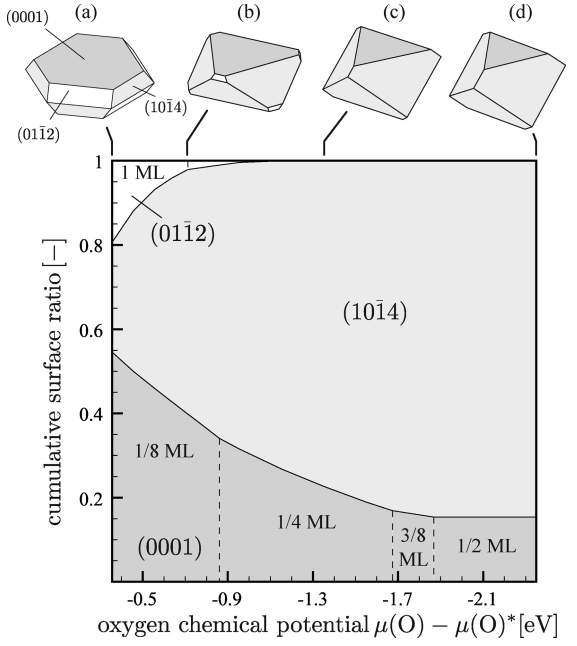

Figure 9. Selected equilibrium shapes of $LiCoO_2$ and relative contribution of each surface as a function the oxygen chemical potential in a Li deficient environment where $LiCoO_2$ is in equilibrium with Co_3O_4.

The phase diagram of Figure 4 shows the respective equilibria that can be achieved. For a lithium deficient setup (i.e., the lithium to cobalt ratio is less than 1:1), equilibria with $LiCo_2O_4$, Co_3O_4, CoO, or Co define the lithium chemical potential as a function of the oxygen chemical potential. In a lithium rich configuration, the equilibria with Li_2O and Li_2O_2 set the relation between oxygen and lithium chemical potential.

The range of crystal shapes that can be generated in a lithium lean system is plotted at the top of Figure 9 for a range of oxygen chemical potentials together with the relative contribution of each surface to the total surface. The equilibrium shapes shown are obtained from the respective surface energies through a Wulff construction, which minimizes the total surface energy for a given particle volume.[9] The equilibrium shapes we find contain only two to three surfaces depending on the oxygen chemical potential. The (10$\bar{1}$4) surface is the only nonpolar surface that is low enough in energy to contribute. The other two nonpolar surfaces do not partake in the formation of the equilibrium crystal due to their significantly larger surface energy. In an oxidizing atmosphere, both polar surfaces contribute to the crystal surface, and the crystal shape is a flat hexagon with the (0001) surface as base and top, respectively. More than 55% of the total surface is occupied by this surface. The remaining 45% are occupied by the (10$\bar{1}$4) and (01$\bar{1}$2) surfaces in roughly the same ratio. Annealing $LiCoO_2$ in an oxidizing atmosphere, hence, leads to a rather unfavorable crystal shape for battery applications that require high rate capability. As the (0001) surface is practically impermeable for lithium ions, only about half the surface can intercalate (deintercalated) ions during discharge (charge), which will lower the rate capability of the material. The surface ratio of the (0001) surface, however, can be reduced by annealing the crystal in a reducing atmosphere. This will increase the surface energy of the (01$\bar{1}$2) and (0001) surfaces, but does not affect the energetics of the (10$\bar{1}$4) surface. Consequently, the relative contribution of the (10$\bar{1}$4) surface will increase. It can be seen from Figure 9 that the (01$\bar{1}$2) surface quickly loses significance if the oxygen chemical potential is lowered, and the particles become thicker as a result of the increasing (0001) surface energy. The corresponding decline of the (0001) surface with oxygen chemical potential decrease is more gradual than that of (01$\bar{1}$2). Nonetheless, its contribution to the total surface area can be reduced to less than 20% in a strongly reducing environment. As a consequence, the crystal shape resembles more a cube (with two cutoff corners) than a flat hexagon under reducing conditions.

Finally, annealing in a slightly Li rich environment might further decrease the contribution of the (0001) surface. For a given oxygen chemical potential, the equilibrium with Li_2O or Li_2O_2 leads to higher lithium chemical potentials than the equilibria with the respective cobalt oxides or metallic cobalt, as can be seen from Figure 4. This translates into a higher energy of the (0001) surface, reducing its contribution to the crystal surface.

Discussion

The equilibrium shape of $LiCoO_2$ is a function of environment. We find that under oxidizing conditions a hexagonal shape is thermodynamically favored, whereas a reducing environment leads to more cubic shapes (with cutoff corners). The (01$\bar{1}$2) surface is thermodynamically stable under oxidizing conditions, but is easily destabilized under more reducing conditions. Also, reducing conditions increase the energy of the (0001) surface leading to thicker particles and a reduction of the surface ratio of this Li impermeable surface. It is the sensitivity of these two polar surfaces toward the environment that alter the equilibrium morphology of the crystal as a function of environment.

A variety of morphologies are reported in the literature as a result of vastly varying syntheses, and it is tempting to comment on some of them in the light of our findings. Carlier et al. obtained $LiCoO_2$ in the O3 host by ion-exchanging Na_xCoO_2 (O2 host) followed by annealing in oxygen.[32] They found different morphologies as a function of annealing temperature. Note that the chemical potential of oxygen will become more negative (i.e., more reducing) with an isobaric increase in temperature. At moderate annealing temperatures (around 400 °C), they report SEM micrographs showing hexagonal particles. However, they obtained a step-like morphology after annealing at 800 °C with top view terraces that resemble the roughly triangular (0001) shape in Figure 9b. Our results indicate that the change in morphology is associated with a tendency to reduce the relative contribution of the (01$\bar{1}$2) surface at lower oxygen chemical potential

(32) Carlier, D.; Saadoune, I.; Croguennec, L.; Menetrier, M.; Suard, E.; Delmas, C. *Solid State Ionics* **2001**, *144*, 263–276.

and, thus, higher annealing temperature. Liang et al. synthesized $LiCoO_2$ in different molten salts at elevated temperatures.[33,34] They observed the formation of flat, polygonal (i.e., approximately hexagonal) crystals. Likewise, Chen and Grey obtained a morphology consisting of intergrown flat, hexagonal crystals from synthesis in a basic melt of mixed-alkali metal salts.[35] Liang et al. also investigated the influence of temperature[33] and found a pronounced growth along one direction with increasing temperature, which they explained based on a kinetic argument. Our results might provide an alternative explanation if the increase in temperature is associated with a shift toward more reducing conditions in the melt, as this would lead to a thickening along [0001] according to Figure 9. More spherical particles were obtained by Sun et al.[36] using a sol−gel synthesis. They calcinated a poly(acrylic acid) (PAA) containing gel precursor, and we speculate that the combustion of PAA and other organic constituents in the precursor during calcination might have created a reducing atmosphere, leading to the observed crystal shape.

The set of identified low-energy surfaces (i.e., (0001), $(10\bar{1}4)$, and $(01\bar{1}2)$) is in reasonable agreement with preferred growth directions of thin-films reported in the literature. The growth behavior of these films is characterized by a competition between surface and strain energy.[37] Hence, one should be careful and draw only loose conclusions with respect to surface energies from the growth behavior of thin films. Nonetheless, observed growth directions of thin films can at least be taken as indicator for surfaces with low energy. Bates et al. used rf magnetron sputtering to grow $LiCoO_2$ films on aluminum and determined the growth direction via XRD.[38] Their work shows that (0001) is the preferred growth direction in the limit of very thin films, where the surface energy should be the dominating factor. This also holds for films produced by other means.[39,40] This is in agreement with our calculations, where the (0001) surface is the lowest energy surface throughout the chemical potential range considered, although the energy of the $(10\bar{1}4)$ surface is comparable under reducing conditions. Furthermore, Bates et al. found that the preferred growth direction changes in favor of $(10\bar{1}1)$ and $(10\bar{1}4)$ with increasing thickness of the film, which can be attributed to less strain energy offsetting the (environment dependent) higher surface energy of these surfaces compared to (0001).[37] In particular, the growth along $(10\bar{1}4)$ is in agreement with our findings. Motivated by their results, we also briefly assessed the energetics of $(10\bar{1}1)$ and found the energy of this polar surface to be higher by about 400−600 mJ/m^2 compared to $(10\bar{1}4)$. This is enough to exclude it from the equilibrium crystal shape (in the range of investigated chemical potentials), but still significantly lower than the energy of $(11\bar{2}0)$ and $(10\bar{1}0)$. They also identified growth along $(01\bar{1}2)$ for thicker films but apparently could not investigate this direction for thinner films because of overlap with a substrate peak in the XRD data.

Undercoordinated Co is energetically unfavorable. This is the main reason for the higher energy of the $(11\bar{2}0)$ and $(10\bar{1}0)$ surfaces compared to the $(10\bar{1}4)$ surface, which excludes them from the equilibrium crystal shape. This is in agreement with earlier investigations of the surface energetics of transition metal phosphates.[19,20] We find the energetic cost to break a Co−O bond at the surface to be about 1 eV per bond. The polar surfaces (i.e., $(01\bar{1}2)$ and (0001)), likewise, favor terminations that minimize coordination loss. Oxygen vacant surface terminations of (0001) stabilize only under highly reducing conditions that cannot be sustained by the bulk material. The $(01\bar{1}2)$ surface contributes significantly to the equilibrium crystal shape only under highly oxidizing conditions, where the surface is terminated by a full ML of oxygens. Under more reducing conditions, the lowest energy configuration for this surface is found by gradually reducing the oxygen coverage. Yet, the energetic cost is so high that the surface quickly loses significance in the Wulff construction.

To stabilize polar surfaces, the surface has to provide charge compensation. This requires a valence change of Co near the surface (cf, Figure 7) for nonstoichiometric configurations. We generally find configurations that imply the oxidation of subsurface Co (i.e., Co^{4+}) energetically less costly than those requiring reduction to Co^{2+}. As a consequence, we find Li deficient ($\leq$1/2 ML) terminations of (0001) to be energetically favorable within the limits of bulk stability. A higher degree of lithium coverage at the (0001) surface would require lithium chemical potentials above the bulk stability region. Likewise, the energy of the $(01\bar{1}2)$ surface can be significantly reduced by oxidizing the surface (i.e., increasing the surface coverage of oxygen beyond 1/2 ML) within the oxygen chemical potential range allowed by the bulk stability. Yet, lowering the surface energy by reducing the surface without losing bulk integrity is strongly limited as it requires highly reducing conditions.

Nonetheless, nonstoichiometric terminations of (0001) and $(01\bar{1}2)$ imply the presence of magnetic subsurface Co. Investigating nanocrystals of $LiCoO_2$, Okubo et al. found an increase in the magnetic susceptibility with decreasing particle size, experimentally corroborating the existence of nondiamagnetic subsurface cobalt.[2] They, however, attributed the change in magnetic susceptibility to the presence of Co^{2+} instead of Co^{4+} after conducting ICP measurements and finding Li excess. Moses et al.,[41] on the

(33) Liang, H.; Qiu, X.; Chen, H.; He, Z.; Zhu, W.; Chen, L. *Electrochem. Commun.* **2004**, *6*, 789–794.
(34) Liang, H.; Qiu, X.; Zhang, S.; He, Z.; Zhu, W.; Chen, L. *Electrochem. Commun.* **2004**, *6*, 505–509.
(35) Chen, H.; Grey, C. P. *Adv. Mater.* **2008**, *20*, 2206–2210.
(36) Sun, Y.; Oh, I.; Hong, S. J. *Mater. Sci.* **1996**, *31*, 3617–3621.
(37) Hart, F.; Bates, J. *J. Appl. Phys.* **1998**, *83*, 7560–7566.
(38) Bates, J.; Dudney, N.; Neudecker, B.; Hart, F.; Jun, H.; Hackney, S. *J. Electrochem. Soc.* **2000**, *147*, 59–70.
(39) Fragnaud, P.; Nagarajan, R.; Schleich, D.; Vujic, D. *J. Power Sources* **1995**, *54*, 362–366.
(40) Julien, C.; Camacho-Lopez, M.; Escobar-Alarcon, L.; Haro-Poniatowski, E. *Mater. Chem. Phys.* **2001**, *68*, 210–216.
(41) Moses, A.; Flores, H.; Kim, J.; Langell, M. *Appl. Surf. Sci.* **2007**, *253*, 4782–4791.

other hand, were not able to detect Co^{2+} by analyzing the Co 2p core peaks of surface sensitive XPS measurements. They did not comment on the possibility of Co^{4+}, probably due to the lower sensitivity of the spectrum toward a change from Co^{3+} to Co^{4+}.[42] Our calculations, in principle, allow for both, yet indicate that surfaces with subsurface Co^{4+} providing charge compensation are better in agreement with bulk stability.

Conclusion

Using first-principles calculations, we investigated the surface energies and equilibrium morphology of $LiCoO_2$. We find that only the (0001), (10$\bar{1}$4), and (01$\bar{1}$2) surfaces show up in the equilibrium shape. The presence of two polar surfaces (i.e., (0001) and (01$\bar{1}$2)), however, is possible only under oxidizing conditions. These surfaces are stabilized by an adjustment of the Co valence near the surface in order to ensure canceling electric fields of the surface layers and global charge balance. The thermodynamically favorable termination depends on the environment, whereby the (01$\bar{1}$2) surface is directly sensitive toward the oxygen chemical potential. In contrast thereto, the (0001) surface termination is a function of the lithium chemical potential and depends on the oxygen chemical potential during annealing only indirectly because of phase equilibria relating both chemical potentials with each other.

The energy of the polar (01$\bar{1}$2) surface increases rather rapidly in more reducing environments, eventually excluding this surface from the equilibrium shape. The energy of the (0001) surface also increases in a reducing environment, diminishing its contribution to the crystal surface. This dependence of the polar surfaces on environment provides the possibility to tailor the contribution of each surface to the crystal. Especially, the reduction of the (0001) surface seems attractive with respect to battery applications, as the surface does not allow for lithium intercalation.

If annealed in an oxidizing environment, the crystal shape is that of a flat hexagon and becomes more cubic in a reducing environment. This allows to reduce the relative surface area of (0001). Thus, we speculate that a synthesis route that provides a reducing environment will lead to a morphology that enhances rate capability. This holds for annealing conditions, but might also be transferred to wet chemistries. In that context, it might be interesting to investigate the effect of pOH in hydrothermal or molten salt synthesis and take the potential into account during electrochemical precipitation.

Acknowledgment. This work was supported by a fellowship within the Postdoc-Programme of the German Academic Exchange Service (DAAD) and by DOE under award number DE-FG02-96ER45571 as well as the National Partnership for Advanced Computational Infrastructure (NPACI).

(42) Daheron, L.; Dedryvere, R.; Martinez, H.; Menetrier, M.; Denage, C.; Delmas, C.; Gonbeau, D. *Chem. Mater.* **2008**, *20*, 583–590.